

## Timeshare surface-enhanced Raman scattering platform with sensitive and quantitative mode

Qianqian Ding\*, Xueyan Chen, Yunlu Jia, Hong Liu, Xiaochen Zhang, Ningtao Cheng\* and Shikuan Yang\*

**Citation:** Ding QQ, Chen XY, Jia YL, Liu H, Zhang XC, Cheng NT, Yang SK. Timeshare surface-enhanced Raman scattering platform with sensitive and quantitative mode. *Opto-Electron Adv* **9**, 250269(2026).

<https://doi.org/10.29026/oea.2026.250269>

Received: 9 October 2025; Accepted: 26 November 2025; Published online: 21 January 2026

### Related articles

Quantitative detection of trace nanoplastics (down to 50 nm) via surface-enhanced Raman scattering based on the multiplex-feature coffee ring

Xiniao Lin, Fengcai Lei, Xiu Liang et al

*Opto-Electronic Advances* 2025, **8**(6): 240260    doi: [10.29026/oea.2025.240260](https://doi.org/10.29026/oea.2025.240260)

Coulomb attraction driven spontaneous molecule-hotspot pairing enables universal, fast, and large-scale uniform single-molecule Raman spectroscopy

Lihong Hong, Haiyao Yang, Jianzhi Zhang et al

*Opto-Electronic Advances* 2025, **8**(7): 240309    doi: [10.29026/oea.2025.240309](https://doi.org/10.29026/oea.2025.240309)

Single-beam optical trap-based surface-enhanced Raman scattering optofluidic molecular fingerprint spectroscopy detection system

Ning Sun, Yuan Gan, Yujie Wu et al

*Opto-Electronic Advances* 2025, **8**(2): 240182    doi: [10.29026/oea.2025.240182](https://doi.org/10.29026/oea.2025.240182)

Enrichment strategies in surface-enhanced Raman scattering: theoretical insights and optical design for enhanced light-matter interaction

Zhiyang Pei, Chang Ji, Mingrui Shao et al

*Opto-Electronic Science* 2025, **4**(12): 250015    doi: [10.29026/oes.2025.250015](https://doi.org/10.29026/oes.2025.250015)

More related articles in Opto-Electronic Journals Group website



# Timeshare surface-enhanced Raman scattering platform with sensitive and quantitative mode

Qianqian Ding<sup>1,2,3\*\*</sup>, Xueyan Chen<sup>1,4†</sup>, Yunlu Jia<sup>1</sup>, Hong Liu<sup>3</sup>, Xiaochen Zhang<sup>1</sup>, Ningtao Cheng<sup>5\*</sup> and Shikuan Yang<sup>1,3\*</sup>

**Abstract:** The sensitivity and quantification capability of surface-enhanced Raman scattering (SERS) substrates are mutually exclusive, because the ultrasensitive SERS sites (hottest spots) necessary for the sensitivity will significantly magnify the SERS signals of the analyte molecules and thus each of these molecules will be miscounted to be hundreds during the quantification process. We demonstrate a concept to circumvent the above contradiction by engineering a timeshare SERS platform capable of working at the quantitative or the sensitive mode on demand. The timeshare SERS platform was constructed by transferring a monolayer gold nanosphere film onto elastic substrates (e.g., hydrogel). The volume change of the hydrogel could adjust the inter-nanosphere distance, dynamically controlling the formation or extinction of the SERS hottest spots on the same SERS substrate without influencing the spatial distribution of the analyte molecules. The timeshare SERS platform without the SERS hottest spots showed strong quantification capability, while when equipped with a substantial number of the SERS hottest spots exhibited ultra-high sensitivity. We demonstrated quantitative and ultrasensitive detection of various analyte molecules using the quantitative and the sensitive mode of the timeshare SERS platform, respectively. We opened an avenue towards designing SERS substrates with both high sensitivity and strong quantification capability.

**Keywords:** timeshare SERS platform; sensing; quantification; hydrogel; gold nanosphere

DOI: [10.29026/oea.2026.250269](https://doi.org/10.29026/oea.2026.250269) | CSTR: [32247.14.oea.2026.250269](https://cstr.cn/32247.14.oea.2026.250269)

**Citation:** Ding QQ, Chen XY, Jia YL et al. Timeshare surface-enhanced Raman scattering platform with sensitive and quantitative mode. *Opto-Electron Adv* 9, 250269 (2026).

## 1 Introduction

Surface-enhanced Raman scattering (SERS) sensing technique characterized by single-molecule sensitivity, fingerprint signals enabled specificity, multiplex detection capability, and water-inactiveness endowed biocompatibility, has promising applications in analytical chemistry, environmental science, food science, and biomedical fields<sup>1–10</sup>. The most sensitive SERS sites (known as hottest spots) located between closely placed (usually < 10 nm) noble metal nanostructures where strong electromagnetic fields exist under laser excitation<sup>11–15</sup>. More than 70% of the SERS intensities arise from < 1% of the analyte molecules located at the

hottest spots<sup>16,17</sup>. Analyte molecules situated at the hottest spots are important to the SERS sensitivity, because one of them can contribute to the SERS intensity hundreds times larger than those located at other locations. The analyte molecules located at the hottest spots will be miscounted to be hundreds of molecules during the quantification process, leading to a poor quantification capability<sup>6,13,16,18</sup>. Because it is almost impossible to deliver all of the analyte molecules to the location with similar electromagnetic field, the SERS sensitivity and quantification capability are mutually exclusive. This intrinsic contradiction makes the construction of SERS platform with both high sensitivity and strong quantification capability very challenging<sup>19–23</sup>.

Received: 9 October 2025

Accepted: 26 November 2025

Published online: 21 January 2026

<sup>1</sup>Department of Medical Oncology, The First Affiliated Hospital, Zhejiang University School of Medicine, Hangzhou 310003, China; <sup>2</sup>Institute of Micro-nano Photonic and Quantum Manipulation, School of Physics, Nanjing University of Science and Technology, Nanjing 210094, China; <sup>3</sup>Institute for Composites Science Innovation, School of Materials Science and Engineering, Zhejiang University, Hangzhou 310027, China; <sup>4</sup>Inner Mongolia Metallic Materials Research Institute, Baotou 014030, China; <sup>5</sup>School of Medicine, Zhejiang University, Hangzhou 310058, China.

<sup>†</sup>These authors contributed equally to this work.

\*Correspondence: QQ Ding, E-mail: [qqding@njust.edu.cn](mailto:qqding@njust.edu.cn); NT Cheng, E-mail: [ncheng@zju.edu.cn](mailto:ncheng@zju.edu.cn); SK Yang, E-mail: [shkyang@zju.edu.cn](mailto:shkyang@zju.edu.cn)

Notably, although elastic SERS substrates with adjustable gaps between neighbouring noble metal nanoparticles have been studied previously<sup>24–29</sup>, they have not been used to construct SERS platforms with both high sensitivity and strong quantification capability. Here we unprecedentedly demonstrated a concept to circumvent the contradiction by designing a timeshare elastic SERS platform equipped with dynamic hot spots capable of switching between the sensitive and the quantitative mode on demand. The concept to construct the timeshare SERS substrate opens a new avenue toward designing SERS sensors with both high sensitivity and strong quantification capability.

## 2 Results and discussion

### 2.1 Fabrication and characterization of the timeshare SERS platform

The timeshare SERS platform consists two critical parts: the gold (Au) nanosphere monolayer and the hydrogel support capable of reversibly and controllably changing its volume (Fig. 1(a)). The self-assembled monolayer Au nanoparticle film is transferred onto the hydrogel support. When the hydrogel support is expanded, the Au nanospheres become loosely packed and the hottest spots disappear according to the finite-difference time-domain (FDTD) simulations (Fig. S1 and Fig. 1(b)), leaving behind the hot spots around isolated Au nanospheres; this is the quantitative sensing mode. When the hydrogel support is shrunk, the Au nanospheres become more closely packed bearing numerous hottest spots within neighbouring Au nanospheres, namely the sensitive mode. The sensitive mode can be used to determine the existence of the analyte molecules of interest and the amount of the analyte molecules can be further evaluated by the quantitative mode of the same SERS substrate.

Before the preparation of the Au nanosphere film, the Au nanospheres with different diameters were first synthesized by a successive seed-mediated growth process<sup>30,31</sup>. 12 nm sized Au nanoparticle seeds were prepared by a chemical

reduction process (Fig. S2). Controlling the amount of Au seeds in the growth solution could prepare different sized Au nanospheres (Fig. S3). Au nanospheres of four different sizes (50 nm, 66 nm, 72 nm, and 104 nm) were prepared. The surface plasmon resonance (SPR) peak of the Au nanospheres gradually redshifted as the size of the nanospheres increased. The densely packed monolayer Au nanosphere film was prepared by a previously reported Marangoni effect-assisted three-phase self-assembly process (Fig. 2(a))<sup>32</sup>. After shaking the mixture of Au nanosphere aqueous colloids and dichloromethane (DCM), Au nanospheres assembled into a film at the water/DCM interface. Slowly introducing *n*-hexane into the mixture transported the assembled Au nanosphere film into the *n*-hexane/water interface (Fig. 2(a)). The formed monolayer nanosphere film demonstrated uniform golden colour, manifesting their well-ordered structure (Fig. 2(b)). The nanosphere films composed of differently sized Au nanospheres were able to be transferred onto any arbitrary substrates (Fig. 2(c)). The nanospheres were hexagonally arranged with a few amounts of defects. Compared with the Au nanosphere colloids, the nanosphere film demonstrated two SPR peaks originating from the SPR (530 nm and 566 nm for 50 nm and 104 nm Au nanospheres, respectively) of individual nanospheres and the plasmonic coupling (704 nm and 760 nm for Au nanosphere film formed by 50 nm and 104 nm Au nanospheres, respectively) between neighbouring nanospheres (Fig. 2(d)). The average gap between neighbouring Au nanospheres in the nanosphere film was less than 2 nm, which can behave as SERS hottest spots<sup>33–36</sup>. Therefore, self-assembled Au nanosphere films have been extensively studied as sensitive SERS substrates<sup>37–41</sup>.

### 2.2 Quantitative capability of the timeshare SERS platform

To evaluate the SERS sensitivity of the densely packed Au nanosphere films, 4-nitrobenzenethiol (4-NBT) was used as the analyte molecule. SERS spectra of Au nanosphere films

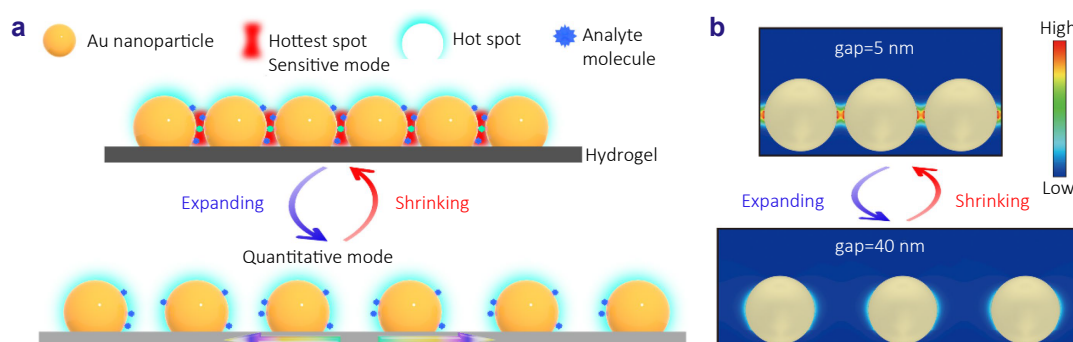


Fig. 1 | The working principle of the timeshare SERS platform equipped with dynamic hot spots, capable of working at the quantitative and the sensitive mode through reversibly swelling and shrinking the hydrogel substrate. (a) Schematic demonstration. (b) FDTD simulation of the electromagnetic field distribution over the Au nanoparticle monolayer film with inter-nanoparticle distances of 5 nm and 40 nm.

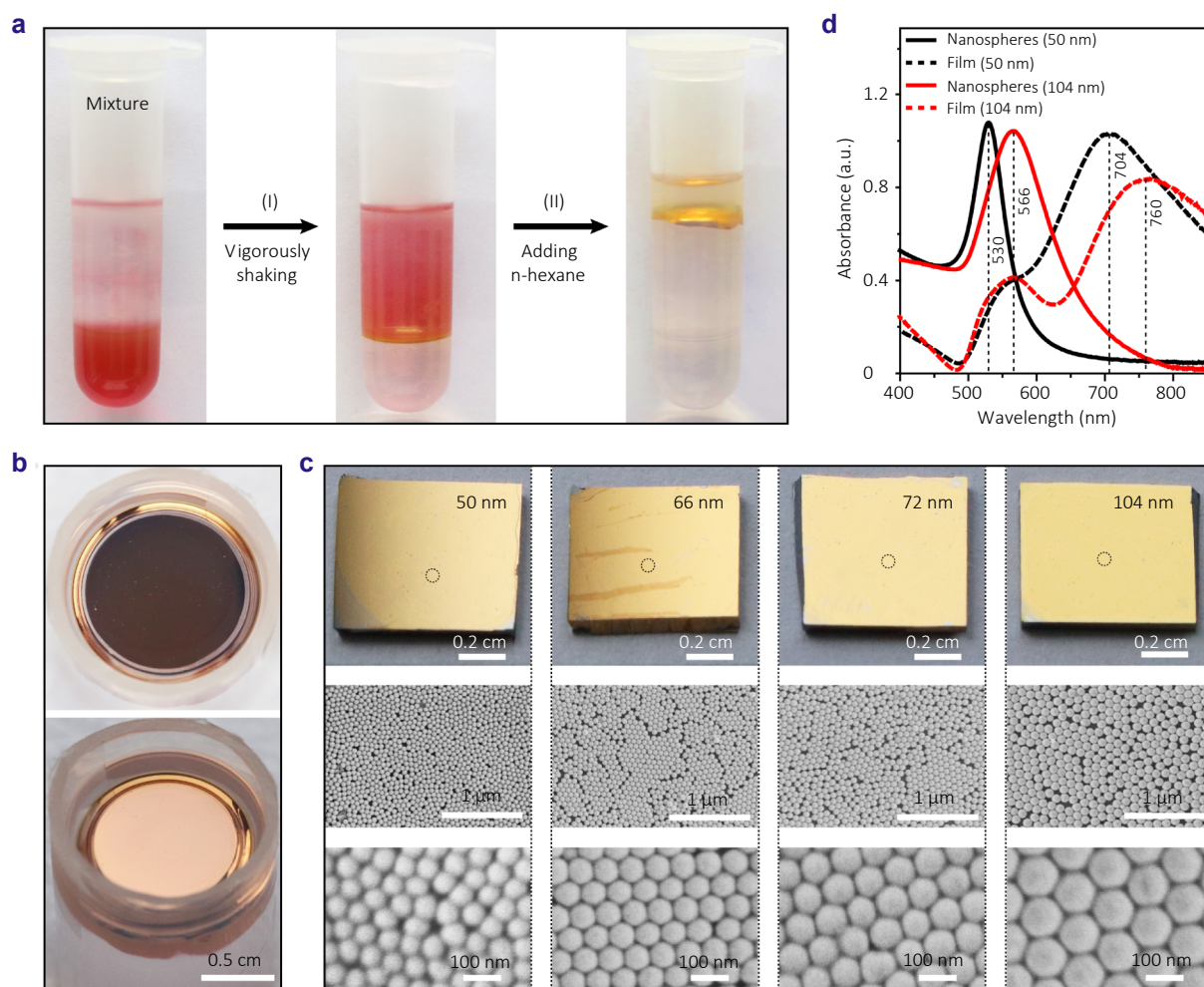


Fig. 2 | Fabrication of large-area Au nanosphere films by a self-assembly process. (a) Photos of the Au nanosphere self-assembly process. Process I. The Au nanosphere colloid was mixed with DCM. Process II. After vigorous shaking, Au nanospheres started to assemble at the water/DCM interface. Process III. Introduction of *n*-hexane transferred the Au nanoparticles to the interface of water and *n*-hexane. (b) Top- and side-view of the assembled Au nanospheres at the water/*n*-hexane interface. (c) Photos of Au nanosphere films composed of differently sized Au nanospheres transferred onto the silicon wafers and the corresponding SEM images at different magnifications (dotted circles marked areas). (d) UV-Vis absorbance spectra of Au nanosphere films composed of 50 nm and 104 nm sized Au nanospheres (dashed lines), and the nanosphere colloids (solid lines).

composed of Au nanospheres with different sizes contaminated by 100 nm 4-NBT ethanol solutions were measured (Fig. S4). The Au nanosphere film composed of 50 nm sized Au nanospheres demonstrated the strongest SERS enhancement under 633 nm laser excitation (Fig. S5). Moreover, the intensity variation of the 1332  $\text{cm}^{-1}$  SERS peak of 4-NBT from the 50 nm sized Au nanospheres formed film was the lowest (relative standard deviation or RSD of the peak intensity equalled 6.5%). Therefore, 50 nm sized Au nanoparticles were chosen in the following experiments.

The other critical part of the timeshare SERS platform is the hydrogel support capable of reversibly and controllably changing its volume. Polyacrylamide (PAAm) hydrogel was used, owing to its excellent ability to swell and shrink<sup>42,43</sup>. The volume of the PAAm hydrogel after swelling could increase by 13 times and the water content reached up to

93% (Fig. S6). The hydrated PAAm hydrogel could be directly used to pick up the freestanding Au nanosphere film at the air/water interface (Fig. 3(a)). After drying naturally, Au nanosphere film was attached onto the hydrogel surface, showing a golden color. The storage performance of the Au nanosphere film/hydrogel composite was characterized. Following preparation, samples were stored at 23 °C and 55% humidity. Volume and color changes during storage are shown in Fig. S7. Within two days, the composite exhibited a 2.82-fold volume decrease accompanied by a surface color change from golden yellow to greenish-yellow. Subsequent measurements revealed a slight volume decrease after one week with no significant change observed for the remaining 120 days (Fig. S8). Scanning electron microscope (SEM) image of the sample preserved for one week showed a reduction in inter-nanosphere distances due to hydrogel

dehydration (Fig. S9). Thereafter, the inter-nanosphere spacing remained stable after one week. Furthermore, the size of the Au nanospheres showed no significant change throughout the 120-day storage. These results demonstrate the good stability of the SERS substrate.

After immersing the Au nanosphere film-covered hydrogel in deionized water (pH = 6.9) at 23 °C for 24 h, the surface area was increased approximately threefold and the golden color evolved into light pink (Fig. 3(b)). The plasmonic coupling peak became very weak, indicating a significant increase in the inter-nanosphere distance due to hydrogel swelling (Fig. 3(c)). SEM images confirmed that the inter-nanosphere distance (> 20 nm) became 10 times larger after volume expansion (inset in Fig. 3(d)). Note that gap variations differ among Au nanospheres of different diameters embedded in the hydrogel. PAAm hydrogels covered with monolayer film formed by 50 nm and 85 nm Au nanospheres were swollen in deionized water at 23 °C and 55% humidity for 24 h. Post-swelling measurements (Fig. S10 and S11) showed average inter-nanosphere spacings of 116.7 nm for 85 nm Au nanosphere monolayer and 74.6 nm

for 50 nm Au nanosphere monolayer, confirming the diameter-dependent expansion of the inter-nanoparticle distance. Factors potentially influencing the variation in gap size include the binding strength between the Au nanospheres and the hydrogel where weak physical adsorption may lead to an uneven gap distribution, as well as temperature, humidity, and solution pH.

The volume of the swollen hydrogel covered by the Au nanospheres was decreased by ~ 80% after immersing in a mixture consisting of water and ethanol at a volume ratio of 1:9 for 24 h at 23 °C and 55% humidity (Fig. 3(b)). The Au nanosphere film on the hydrogel surface turned back to the golden color. A strong SPR peak at 657 nm originating from the plasmonic coupling between closely packed Au nanospheres appeared (Fig. 3(c)). SEM observations revealed the extremely narrow gap between neighbouring Au nanospheres (Fig. 3(e)). Wrinkles were formed within the Au nanoparticle film because the hydrogel shrunk smaller than the time when the Au nanoparticle film was transferred (Fig. 3(a)). In short, the inter-nanosphere distance could be dynamically controlled by the PAAm

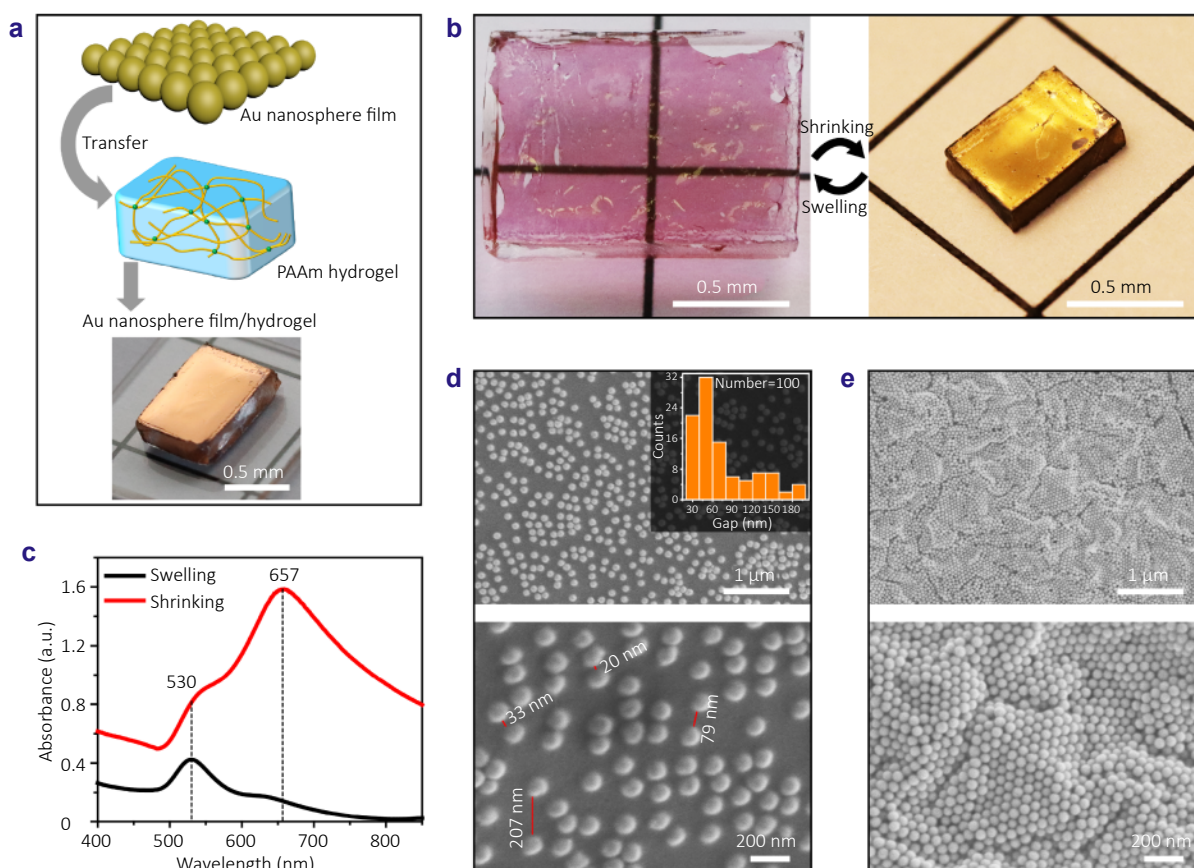


Fig. 3 | Timeshare SERS platform. (a) Schematic of the preparation process of the timeshare SERS platform formed by Au nanosphere film-covered PAAm hydrogel. (b) The dynamic volumetric and colour change of the timeshare SERS platform induced by the swelling or shrinking of the hydrogel. (c) UV-Vis absorbance spectra of the timeshare SERS platform after swelling and shrinking the hydrogel support. (d) and (e) SEM images of the Au nanosphere film attached on the hydrogel support after swelling and shrinking the hydrogel, respectively. Inset in (d): distribution of the inter-nanosphere after swelling the hydrogel support.

hydrogel substrate, endowing the dynamic SERS hot spots to the SERS platform.

We first evaluated the quantitative capability of the timeshare SERS platform when the PAAm hydrogel was at the swollen state using 4-NBT as a model molecule (Fig. 4(a–f)). The intensity of the SERS signals of 4-NBT molecules gradually decreased as the concentration of 4-NBT solution was reduced (Fig. 4(a)). The lowest detection concentration was as low as 0.5 nM (Fig. S12). The relationship between the concentration of 4-NBT solutions and the intensity of the 1332  $\text{cm}^{-1}$  SERS peak could be described by  $\log C = 2.08 \log I - 14.65$  with  $R^2$  (goodness of fit) equaled 0.9902 (Fig. 4(b)). Moreover, the SERS mapping results at different concentrations of 4-NBT solutions exhibited a uniform color, indicating the small SERS intensity fluctuations (Fig. 4(c, d) and Fig. S13(a–c)). Additionally, the RSD of the SERS intensity at 1332  $\text{cm}^{-1}$  of 4-NBT at different concentrations were less than 10% (Fig. 4(e) and 4(f) and Fig. S13(d–f)). The high  $R^2$  and the low RSD values proved the strong quantification capability of the timeshare SERS platform at the swollen state, originating from the absence of SERS hottest spots and all the analyte molecules were situated at the place with similar electromagnetic field strength.

Immersing the hydrogel in a mixture of water and ethanol could shrink the volume of the hydrogel to create SERS hottest spots between neighbouring Au nanospheres, enabling the timeshare SERS platform to work at the sensitive mode. The analyte molecules located at the orbital of the Au nanospheres at the quantitative mode now exposed to the SERS hottest spots, which could significantly contribute to the SERS signals (Fig. 1). As anticipated, strong SERS signals of 4-NBT at different concentrations were clearly observed on the shrunk SERS platform (Fig. 4(g)). The SERS signals of 4-NBT molecules at 0.01 nM were still reliably observable; in contrast, the SERS platform working at quantitative mode could only reliably detect 4-NBT molecules at 1 nM. The lowest detection concentration of 4-NBT was down to 100 fM by the SERS mapping measurements (Fig. S14). The sensitivity of the timeshare SERS platform working at the sensitive mode is better than most of the previous publications<sup>25,44–46</sup>. The relationship between the concentration of 4-NBT solutions and the SERS intensity at 1332  $\text{cm}^{-1}$  could be described by  $\log C = 2.56 \log I - 17.49$  with  $R^2$  equalled 0.9668 (Fig. 4(h)). Compared to the quantitative mode, the SERS mapping measurements displayed obvious SERS intensity fluctuations (Fig. 4(i) and 4(j), and Fig. S15(a–c)). The RSD values of the SERS intensity at 1332  $\text{cm}^{-1}$  were more than 25%, much higher than the quantitative mode (Fig. 4(k) and 4(l), and Fig. S15(d–f)). The observed low  $R^2$  and high RSD values are attributed to the emergence of SERS hottest spots between adjacent Au nanospheres and hotspot clustering phenomena. In terms of sensitivity and quantitative analysis capabilities, our timeshare SERS platform performs comparably to the three-dimensional Ag/Au nanoparticle-hydrogel composite SERS substrates<sup>47,48</sup>, as

shown in Table S1.

Furthermore, the cycling stability of the timeshare SERS platform was evaluated over multiple swelling-shrinking cycles. SERS spectra of 500 nM 4-NBT adsorbed on Au nanosphere film/hydrogel composites were acquired over 10 consecutive swelling-shrinking cycles at 23 °C and 55% humidity, as shown in Fig. S16(a). The SERS intensity of the 1332  $\text{cm}^{-1}$  peak decreased by 23% after 5 swelling-shrinking cycles and 38% after 10 swelling-shrinking cycles (Fig. S16(b)). This signal attenuation is primarily attributable to partial desorption of 4-NBT molecules during repeated volumetric changes. On the other hand, the influence of environmental factors (humidity and temperature) was also examined. SERS spectra acquired at different swelling temperatures (constant shrinking at 23 °C, 55% humidity) showed no significant temperature dependence in the 1332  $\text{cm}^{-1}$  peak intensity (Fig. S17). Conversely, SERS performance exhibited strong humidity dependence (Fig. S18), driven by the humidity-sensitive equilibrium swelling degree of PAAm hydrogel. At 85% humidity, maximal hydrogel swelling enhanced the adsorption capacity for 4-NBT molecules, yielding a 24% increase in SERS intensity at 1332  $\text{cm}^{-1}$  compared to measurements at 55% humidity. Therefore, optimizing humidity is essential to maximizing SERS signal intensity.

### 2.3 Quantitative and sensitive detection for biomolecules by the timeshare SERS platform

As anticipated, the timeshare SERS platform could work at the quantitative and the sensitive mode. We consequently investigated the application of the timeshare SERS platform in biomolecule detection and quantification. Adenosine has been reported to play a crucial role in the regulation of physiological activity in various tissues and organs, which is also a cancer biomarker<sup>49,50</sup>. We first determined the quantity of adenosine using the quantification capability of the timeshare SERS platform (Fig. 5(a)). The characteristic SERS peak at 735  $\text{cm}^{-1}$  assigned to the ring breathing mode of adenosine was clearly observed in the concentration range of 10 nM to 100  $\mu\text{M}$ . The relationship between the SERS peak intensity at 735  $\text{cm}^{-1}$  and the concentration could be described by  $\log C = 3.03 \log I - 16.76$  with  $R^2$  equalled 0.9707 (Fig. 5(b)). The lowest detection concentration of adenosine using the timeshare SERS platform at the quantification mode could reach 5 nM (Fig. S19). After shrinking the hydrogel to make the timeshare SERS platform work at the sensitivity mode, the SERS peak intensity was greatly enhanced (Fig. 5(c)). Even the concentration of adenosine was down to 10 pM, the SERS peaks were still observable, better than most of the previously reported results<sup>49,51</sup>. The relationship between the concentration of adenosine and the SERS intensity at 735  $\text{cm}^{-1}$  could be described by  $\log C = 3.70 \log I - 20.15$  with a greatly reduced  $R^2$  of 0.9244 (Fig. 5(d)).

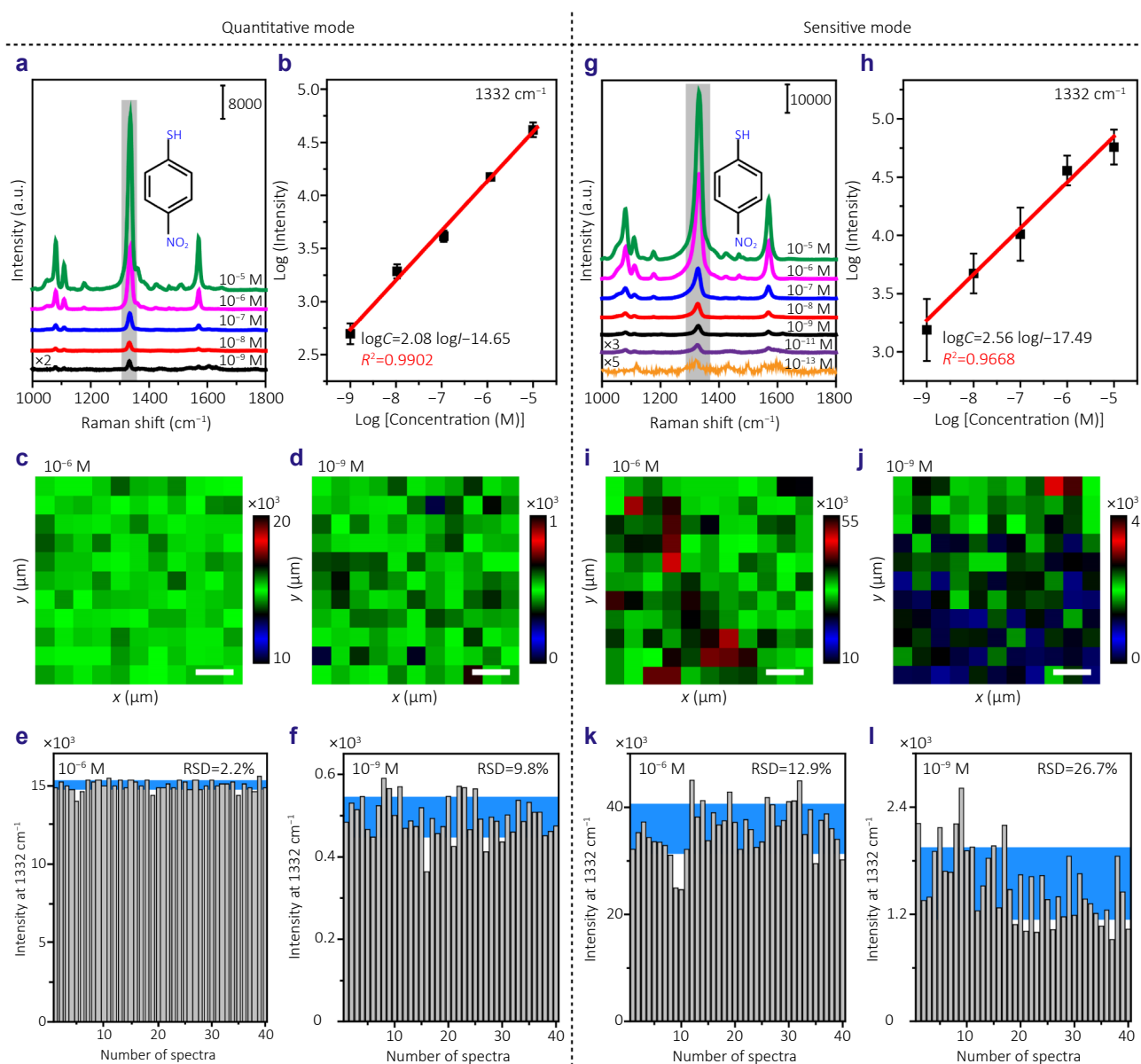


Fig. 4 | Characterization of the quantitative and the sensitive mode of the timeshare SERS platform. (a) Typical SERS spectra of 4-NBT at different concentrations enhanced by the Au nanospheres on the swollen hydrogel (i.e., quantitative mode). Inset: molecular structure of 4-NBT. (b) The relationship between the intensity of the Raman band at  $1332\text{ cm}^{-1}$  and the concentrations of 4-NBT under the quantitative mode. (c) and (d) SERS mapping results of the Raman band at  $1332\text{ cm}^{-1}$  of 4-NBT at different concentration under the quantitative mode. (e, f) RSD of the intensity of the  $1332\text{ cm}^{-1}$  SERS peak of 4-NBT at different concentrations under the quantitative mode. (g) Typical SERS spectra of 4-NBT at different concentrations enhanced by the closely packed Au nanospheres on the shrunk hydrogel (i.e., sensitive mode). (h) The relationship between the intensity of the Raman band at  $1332\text{ cm}^{-1}$  and the concentrations of 4-NBT under the sensitive mode. (i, j) SERS mapping results of the Raman band at  $1332\text{ cm}^{-1}$  of 4-NBT at different concentrations under the sensitive mode. (k, l) RSD of the intensity of the  $1332\text{ cm}^{-1}$  SERS peak of 4-NBT at different concentrations under the sensitive mode. Error bars were obtained based on 40 SERS spectra.

Adenine is one of the aromatic bases of DNA and RNA. Quantitative and highly sensitive detection of adenine are desirable for the detection of diseases, DNA hybridization monitoring, and other biomedical applications<sup>52,53</sup>. The relationship between the SERS peak at  $736\text{ cm}^{-1}$  and the concentration of adenine in the range of  $100\text{ }\mu\text{M}$  to  $10\text{ nM}$  could be described by  $\log C = 2.38 \log I - 14.69$  with  $R^2$  equaled  $0.9849$

(Fig. 5(e) and 5(f)). The uniform color of the SERS mapping images of  $736\text{ cm}^{-1}$  SERS peak at different concentrations reflected the detection reliability using the timeshare SERS platform working under the quantitative mode (Fig. S20). The corresponding RSD values at different concentrations were less than 10%, further proved the detection reliability at the quantification mode (Fig. S21).

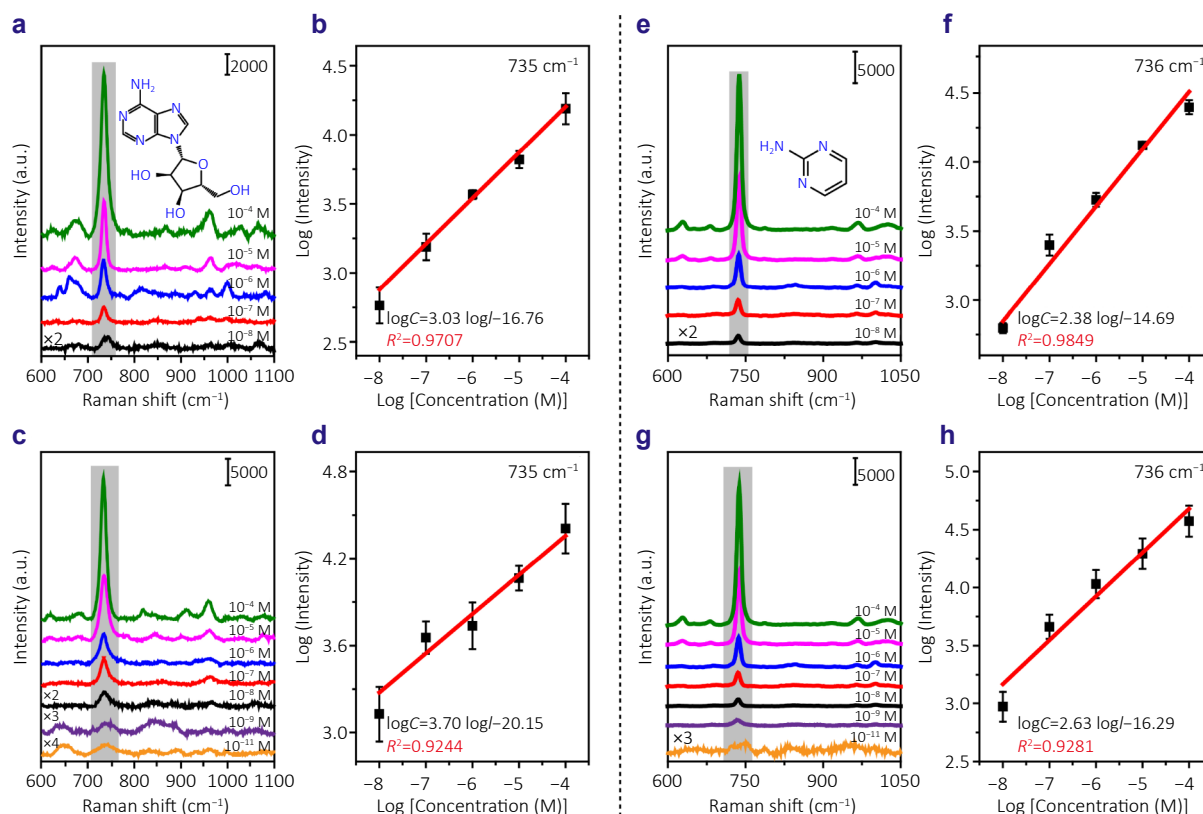


Fig. 5 | Quantitative and sensitive detection for biomolecules by the timeshare SERS platform. (a) SERS spectra of adenosine at different concentrations enhanced by the Au nanospheres on the swollen hydrogel (i.e., quantitative mode). Inset: molecular structure of adenosine. (b) The relationship between the intensity of the Raman band at  $735\text{ cm}^{-1}$  and the concentrations of adenosine under the quantitative mode. (c) SERS spectra of adenosine at different concentrations enhanced by the closely packed Au nanospheres on the shrunken hydrogel (i.e., sensitive mode). (d) The relationship between the intensity of the Raman band at  $735\text{ cm}^{-1}$  and the concentrations of adenosine under the sensitive mode. (e) SERS spectra of adenine at different concentrations enhanced by the Au nanospheres on the swollen hydrogel (i.e., quantitative mode). Inset: molecular structure of adenine. (f) The relationship between the intensity of the Raman band at  $736\text{ cm}^{-1}$  and the concentrations of adenine under the quantitative mode. (g) SERS spectra of adenine at different concentrations enhanced by the closely packed Au nanospheres on the shrunken hydrogel (i.e., sensitive mode). (h) The relationship between the intensity of the Raman band at  $735\text{ cm}^{-1}$  and the concentrations of adenine under the sensitive mode. Error bars were obtained based on 40 SERS spectra.

The SERS signals of adenine at different concentrations were significantly enhanced when the hydrogel substrate was shrunken (Fig. 5(g)). The lowest detection concentration of adenine reached  $10\text{ pM}$ , improved by two orders of magnitudes than the quantification mode (Fig. S22). The relationship between the concentration in the range of  $100\text{ }\mu\text{M}$  to  $10\text{ nM}$  and the SERS intensity at  $736\text{ cm}^{-1}$  could be described by  $\log C = 2.63 \log I - 16.29$  with a greatly reduced  $R^2$  of 0.9281. The SERS mapping results exhibited obvious SERS intensity fluctuations (Fig. S23), and the corresponding RSD values were more than 10% (Fig. S24). These results proved the poor detection reliability but high sensitivity of the timeshare SERS platform at sensitive mode.

### 3 Conclusions

We demonstrated a timeshare SERS platform capable of working at the quantitative and the sensitive mode on demand at desired times, which circumvented the inherent

contradiction between the quantification and the sensitivity of conventional SERS substrates. The timeshare SERS platform could be used to reliably quantify specific analytes; if no SERS signals of the analyte were observed, then the timeshare SERS platform could be switched to the sensitive mode to confirm the existence/absence of the analytes, or vice versa. The limitations and potential improvements for the timeshare SERS platform primarily involve two key aspects: i) Enhancing detection sensitivity through the implementation of high-enhancement plasmonic nanostructures (e.g., 2D Au trisoctahedron or triangular nanoprisms); ii) Addressing material stability issues: organic solvents (such as alcohols, acetone) can disrupt the swelling equilibrium of the PAAm hydrogel, while acidic or alkaline media induce hydrolysis and cleavage of its amide bonds. Consequently, the current restriction to aqueous detection necessitates the development of composite hydrogel systems to expand the range of applicable sample types. In conclusion, the timeshare SERS platform would have promising applications in

the broad fields where there is urgent need for both quantitative and sensitive detections of trace amounts of analytes.

## References

1. Homola J. Surface plasmon resonance sensors for detection of chemical and biological species. *Chem Rev* **108**, 462–493 (2008).
2. Li JF, Huang YF, Ding Y et al. Shell-isolated nanoparticle-enhanced Raman spectroscopy. *Nature* **464**, 392–395 (2010).
3. Bodelón G, Montes-García V, López-Puente V et al. Detection and imaging of quorum sensing in *Pseudomonas aeruginosa* biofilm communities by surface-enhanced resonance Raman scattering. *Nat Mater* **15**, 1203–1211 (2016).
4. Langer J, de Aberasturi DJ, Aizpurua J et al. Present and future of surface-enhanced Raman scattering. *ACS Nano* **14**, 28–117 (2020).
5. Yang SK, Dai XM, Stogin BB et al. Ultrasensitive surface-enhanced Raman scattering detection in common fluids. *Proc Natl Acad Sci USA* **113**, 268–273 (2016).
6. Lee HK, Lee YH, Koh CSL et al. Designing surface-enhanced Raman scattering (SERS) platforms beyond hotspot engineering: emerging opportunities in analyte manipulations and hybrid materials. *Chem Soc Rev* **48**, 731–756 (2019).
7. Chen XY, Ding QQ, Bi C et al. Lossless enrichment of trace analytes in levitating droplets for multiphase and multiplex detection. *Nat Commun* **13**, 7807 (2022).
8. Bi XY, Czajkowsky DM, Shao ZF et al. Digital colloid-enhanced Raman spectroscopy by single-molecule counting. *Nature* **628**, 771–775 (2024).
9. Pei ZY, Ji C, Shao M et al. Enrichment strategies in surface-enhanced Raman scattering: theoretical insights and optical design for enhanced light-matter interaction. *Opto-Electron Sci* **4**, 250015 (2025).
10. Wu Y, Sun TY, Shao MR et al. Pyroelectrically driven charge transfer and its advantages on SERS and self-cleaning property. *Laser Photon Rev* **19**, 2401152 (2025).
11. Nie SM, Emory SR. Probing single molecules and single nanoparticles by surface-enhanced Raman scattering. *Science* **275**, 1102–1106 (1997).
12. Lim DK, Jeon KS, Hwang JH et al. Highly uniform and reproducible surface-enhanced Raman scattering from DNA-tailorable nanoparticles with 1-nm interior gap. *Nat Nanotechnol* **6**, 452–460 (2011).
13. Chen HY, Lin MH, Wang CY et al. Large-scale hot spot engineering for quantitative sers at the single-molecule scale. *J Am Chem Soc* **137**, 13698–13705 (2015).
14. Benz F, Schmidt MK, Dreismann A et al. Single-molecule optomechanics in "picocavities". *Science* **354**, 726–729 (2016).
15. Sun HY, He Y, Qiao SD et al. Highly sensitive and real-simultaneous CH<sub>4</sub>/C<sub>2</sub>H<sub>2</sub> dual-gas LITES sensor based on Lissajous pattern multi-pass cell. *Opto-Electron Sci* **3**, 240013 (2024).
16. Fang Y, Seong NH, Dlott DD. Measurement of the distribution of site enhancements in surface-enhanced Raman scattering. *Science* **321**, 388–392 (2008).
17. Ding QQ, Wang J, Chen XY et al. Quantitative and sensitive SERS platform with analyte enrichment and filtration function. *Nano Lett* **20**, 7304–7312 (2020).
18. Cang H, Labno A, Lu CG et al. Probing the electromagnetic field of a 15-nanometre hotspot by single molecule imaging. *Nature* **469**, 385–388 (2011).
19. Bell SEJ, Sirimuthu NMS. Quantitative surface-enhanced Raman spectroscopy. *Chem Soc Rev* **37**, 1012–1024 (2008).
20. Lee HK, Lee YH, Phang IY et al. Plasmonic liquid marbles: a miniature substrate-less sers platform for quantitative and multiplex ultra-trace molecular detection. *Angew Chem Int Ed* **53**, 5054–5058 (2014).
21. Qiao XZ, Su BS, Liu C et al. Selective surface enhanced Raman scattering for quantitative detection of lung cancer biomarkers in superparticle@MOF structure. *Adv Mater* **30**, 1702275 (2018).
22. Tian L, Su MK, Yu FF et al. Liquid-state quantitative SERS analyzer on self-ordered metal liquid-like plasmonic arrays. *Nat Commun* **9**, 3642 (2018).
23. Bell SEJ, Charron G, Cortés E et al. Towards reliable and quantitative surface-enhanced Raman scattering (SERS): from key parameters to good analytical practice. *Angew Chem Int Ed* **59**, 5454–5462 (2020).
24. Manikas AC, Romeo G, Papa A et al. Highly efficient surface-enhanced Raman scattering substrate formulation by self-assembled gold nanoparticles physisorbed on poly(*N*-isopropylacrylamide) thermoresponsive hydrogels. *Langmuir* **30**, 3869–3875 (2014).
25. Men DD, Liu GQ, Xing CC et al. Dynamically tunable plasmonic band for reversible colorimetric sensors and surface-enhanced Raman scattering effect with good sensitivity and stability. *ACS Appl Mater Interfaces* **12**, 7494–7503 (2020).
26. Li HL, Men DD, Sun YQ et al. Surface enhanced Raman scattering properties of dynamically tunable nanogaps between Au nanoparticles self-assembled on hydrogel microspheres controlled by pH. *J Colloid Interface Sci* **505**, 467–475 (2017).
27. Bharati MSS, Soma VR. Flexible SERS substrates for hazardous materials detection: recent advances. *Opto-Electron Adv* **4**, 210048 (2021).
28. Chen MM, Liu ZH, Su BH et al. High-performance hydrogel SERS chips with tunable localized surface plasmon resonance for coordinated electromagnetic enhancement with chemical enhancement. *Adv Opt Mater* **11**, 2202852 (2023).
29. Wang X, Shen S, Sun N et al. Neural network-assisted dual-functional hydrogel-based microfluidic sers sensing for divisional recognition of multimolecule fingerprint. *ACS Sens* **10**, 1197–1205 (2025).
30. Zheng YQ, Zhong XL, Li ZY et al. Successive, seed-mediated growth for the synthesis of single-crystal gold nanospheres with uniform diameters controlled in the range of 5–150 nm. *Part Part Syst Charact* **31**, 266–273 (2014).
31. Yoon S, Kim C, Lee B et al. From a precursor to an etchant: spontaneous inversion of the role of Au(III) chloride for one-pot synthesis of smooth and spherical gold nanoparticles. *Nanoscale Adv* **1**, 2157–2161 (2019).
32. Lin X, Fang GQ, Liu YL et al. Marangoni effect-driven transfer and compression at three-phase interfaces for highly reproducible nanoparticle monolayers. *J Phys Chem Lett* **11**, 3573–3581 (2020).
33. Qin LD, Zou SL, Xue C et al. Designing, fabricating, and imaging Raman hot spots. *Proc Natl Acad Sci USA* **103**, 13300–13303 (2006).
34. Zhao K, Troparevsky MC, Xiao D et al. Electronic coupling and optimal gap size between two metal nanoparticles. *Phys Rev Lett* **102**, 186804 (2009).
35. Lim DK, Jeon KS, Kim HM et al. Nanogap-engineerable Raman-active nanodumbbells for single-molecule detection. *Nat Mater* **9**, 60–67 (2010).
36. Xing CC, Liu DL, Chen JX et al. Convective self-assembly of 2D nonclose-packed binary Au nanoparticle arrays with tunable optical properties. *Chem Mater* **33**, 310–319 (2021).
37. Lu Y, Liu GL, Lee LP. High-density silver nanoparticle film with temperature-controllable interparticle spacing for a tunable surface enhanced Raman scattering substrate. *Nano Lett* **5**, 5–9 (2005).
38. Wang H, Levin CS, Halas NJ. Nanosphere arrays with controlled sub-10-nm gaps as surface-enhanced Raman spectroscopy substrates. *J Am Chem Soc* **127**, 14992–14993 (2005).
39. Cecchini MP, Turek VA et al. Self-assembled nanoparticle arrays for multiphase trace analyte detection. *Nat Mater* **12**, 165–171 (2013).

40. Liu K, Bai YC, Zhang L et al. Porous Au-Ag nanospheres with high-density and highly accessible hotspots for SERS analysis. *Nano Lett* **16**, 3675–3681 (2016).
41. Si SR, Liang WK, Sun YH et al. Facile fabrication of high-density sub-1-nm gaps from Au nanoparticle monolayers as reproducible SERS substrates. *Adv Funct Mater* **26**, 8137–8145 (2016).
42. Chen F, Tillberg PW, Boyden ES. Expansion microscopy. *Science* **347**, 543–548 (2015).
43. Oran D, Rodrigues SG, Gao RX et al. 3D nanofabrication by volumetric deposition and controlled shrinkage of patterned scaffolds. *Science* **362**, 1281–1285 (2018).
44. Contreras-Cáceres R, Abalde-Cela S, Guardia-Girós P et al. Multifunctional microgel magnetic/optical traps for SERS ultradetection. *Langmuir* **27**, 4520–4525 (2011).
45. Mengesha ZT, Yang J. Silver nanoparticle-decorated shape-memory polystyrene sheets as highly sensitive surface-enhanced Raman scattering substrates with a thermally inducible hot spot effect. *Anal Chem* **88**, 10908–10915 (2016).
46. Song JE, Kim H, Lee SW et al. Nanoscale structural switching of plasmonic nanograin layers on hydrogel colloidal monolayers for highly sensitive and dynamic SERS in water with areal signal reproducibility. *Anal Chem* **89**, 11259–11268 (2017).
47. Xing CC, Zhong SC, Liu DL et al. Hydrogel film@Au nanoparticle arrays based on self-assembly Co-assisted by electrostatic attraction and hydrogel-shrinkage for SERS detection with active gaps. *Adv Mater Interfaces* **8**, 2101055 (2021).
48. Chen MM, Zhang JX, Zhu XJ et al. Hybridizing silver nanoparticles in hydrogel for high-performance flexible SERS chips. *ACS Appl Mater Interfaces* **14**, 26216–26224 (2022).
49. Yang TX, Guo XY, Wu YP et al. Facile and label-free detection of lung cancer biomarker in urine by magnetically assisted surface-enhanced Raman scattering. *ACS Appl Mater Interfaces* **6**, 20985–20993 (2014).
50. García-Astrain C, Lenzi E, de Aberasturi DJ et al. 3D-printed biocompatible scaffolds with built-in nanoplasmonic sensors. *Adv Funct Mater* **30**, 2005407 (2020).
51. Xu SC, Man BY, Jiang SZ et al. Graphene/Cu nanoparticle hybrids fabricated by chemical vapor deposition as surface-enhanced Raman scattering substrate for label-free detection of adenosine. *ACS Appl Mater Interfaces* **7**, 10977–10987 (2015).
52. Tzeng Y, Lin BY. Silver-based SERS pico-molar adenine sensor. *Biosensors* **10**, 122 (2020).
53. Sivaprakasam V, Hart MB. Surface-enhanced Raman spectroscopy for environmental monitoring of aerosols. *ACS Omega* **6**, 10150–10159 (2021).

## Acknowledgements

This work was supported by the National Science Foundation of China (12304422, 52501261, 52273233), the China Postdoctoral Science Foundation (512200-X92103), the Natural Science Foundation of Jiangsu Province (BK20230911), the fundamental Research Funds for the Central Universities (30923010209) and Natural Science Foundation of Inner Mongolia (2025QN05053).

## Author contributions

Q. Q. Ding, Y. Chen and S. K. Yang conceived the idea and supervised the research. S. K. Yang and N. T. Cheng supervised the project. Q. Q. Ding, X. Y. Chen and H. Liu fabricated the samples and performed the measurements. Y. L. Jia provide the assistance with medical applications. All authors commented on the manuscript. Qianqian Ding, Xueyan Chen, Yunlu Jia contributed equally to this work.

## Competing interests

The authors declare no competing financial interests.

## Supplementary information

Supplementary information for this paper is available at <https://doi.org/10.29026/oea.2026.250269>



**Open Access** This article is licensed under a Creative Commons Attribution 4.0 International License, which permits use, sharing, adaptation, distribution and reproduction in any medium or format, as long as you give appropriate credit to the original author(s) and the source, provide a link to the Creative Commons license, and indicate if changes were made. To view a copy of this license, visit <http://creativecommons.org/licenses/by/4.0/>

©The Author(s) 2026.

Published by Editorial Office of *Opto-Electronic Advance*, Institute of Optics and Electronics, Chinese Academy of Sciences.

